J|A|C|S
ARTICLES
Published on Web 06/06/2002

Long-Range Electron Transfer across Molecule−Nanocrystalline Semiconductor Interfaces Using Tripodal Sensitizers

Elena Galoppini,*,† Wenzhuo Guo,† Wei Zhang,† Paul G. Hoertz,‡ Ping Qu,‡ and Gerald J. Meyer*,‡

Contribution from the Chemistry Department, Rutgers University, 73 Warren Street, Newark, New Jersey 07102, and Department of Chemistry, Johns Hopkins University, 3400 North Charles Street, Baltimore, Maryland 21218

Received February 6, 2002

Abstract: Four tripodal sensitizers, $Ru(bpy)_2(Ad\text{-}tripod\text{-}phen)^{2+}$ (**1**), $Ru(bpy)_2(Ad\text{-}tripod\text{-}bpy)^{2+}$ (**2**), $Ru(bpy)_2(C\text{-}tripod\text{-}phen)^{2+}$ (**3**), and $Ru(bpy)_2(C\text{-}tripod\text{-}bpy)^{2+}$ (**4**) (where bpy is 2,2′-bipyridine, phen is 1,10-phenanthroline, and Ad-tripod-bpy (phen) and C-tripod-bpy (phen) are tripod-shaped bpy (phen) ligands based on 1,3,5,7-tetraphenyladamantane and tetraphenylmethane, respectively), have been synthesized and characterized. The tripodal sensitizers consist of a rigid-rod arm linked to a Ru^{II}-polypyridine complex at one end and three COOR groups on the other end that bind to metal oxide nanoparticle surfaces. The excited-state and redox properties of solvated and surface-bound **1**−**4** have been studied at room temperature. The absorption spectra, emission spectra, and electrochemical properties of **1**−**4** in acetonitrile solution are preserved when **1**−**4** are bound to nanocrystalline (anatase) TiO_2 or colloidal ZrO_2 mesoporous films. This behavior is indicative of weak electronic coupling between TiO_2 and the sensitizer. The kinetics for excited-state decay are exponential for **1**−**4** in solution and are nonexponential when **1**−**4** are bound to ZrO_2 or TiO_2. Efficient and rapid ($k_{cs} > 10^8\ s^{-1}$) excited-state electron injection is observed for **1**−**4**/TiO_2. The recombination of the injected electron with the oxidized Ru^{III} center is well described by a second-order kinetic model with rate constants that are independent of the sensitizer. The sensitizers bound to TiO_2 were reversibly oxidized electrochemically with an apparent diffusion coefficient $\sim 1 \times 10^{-11}\ cm^2\ s^{-1}$.

Introduction

Interest in nanometer-sized semiconductor surfaces has risen as the tendency toward miniaturization in the electronic industry continues. The covalent attachment of redox-active and photoactive molecules to semiconductor surfaces is an important step toward the development of molecular devices, such as solar cells, light-emitting diodes, and chemical sensors.[1] Thus, fundamental studies of electronic interactions across molecule−nanoparticle interfaces are increasingly relevant in several emerging fields of science.[2]

The sensitization of nanocrystalline titanium dioxide to visible light with dye molecules is a field in which tuning molecular−semiconductor interactions could lead to improvements and further insights.[3] For example, Figure 1a shows some key electronic transitions that promote and inhibit light energy conversion at a nanocrystalline (anatase) TiO_2 interface with $Ru(dcb)(bpy)_2^{2+}$, where dcb is 4,4′-$(COOH)_2$-2,2-bipyridine. Photoexcitation of the Ru^{II} complex results in the formation of metal-to-ligand charge-transfer (MLCT) excited states that can inject electrons into TiO_2 to form an interfacial charge-separated state consisting of an electron in TiO_2 and an oxidized dye ($Ru^{III}|TiO_2(e^-)$). It has been shown that under a wide variety of experimental conditions the injection yield is near unity and the injection can occur on an ultrafast femtosecond time scale.[3]

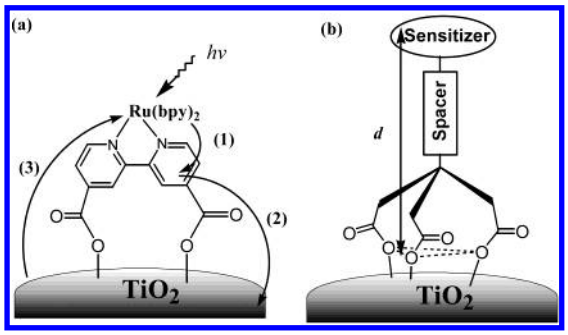

Figure 1. **(a)** Main steps in the sensitization of TiO_2 by a surface-bound Ru^{II}-polypyridyl complex: (1) MLCT excitation; (2) charge separation; and (3) charge recombination. **(b)** Schematic representation of a surface-bound molecular tripodal sensitizer, where *d* is the distance from the Ru center to the footprint, i.e., the plane defined by the three surface-bound oxygen atoms and shown as a dotted line.

* To whom corresponcence should be addressed. E-mail: galoppin@andromeda.rutgers.edu.
† Rutgers University.
‡ Johns Hopkins University.

(1) (a) *Molecular Electronics*; Jortner, J., Ratner, M., Eds.; Blackwell: London, 1997. (b) Meyer, G. J. *Molecular Level Artificial Photosynthetic Materials*; Progress in Inorganic Chemistry; John Wiley & Sons: New York, 1997.
(2) Alivisatos, A. P. *J. Phys. Chem.* **1996**, *100*, 13226.
(3) (a) Hagfeldt, A.; Grätzel, M. *Chem. Rev.* **1995**, *95*, 49. (b) Kamat, P. V. *Chem. Rev.* **1993**, *93*, 267. (c) Qu, P.; Meyer, G. J. In *Electron Transfer in Chemistry*; Balzani, V., Ed.; Wiley: New York, 2001; Vol. IV, Part 2, Chapter 2, p 355.

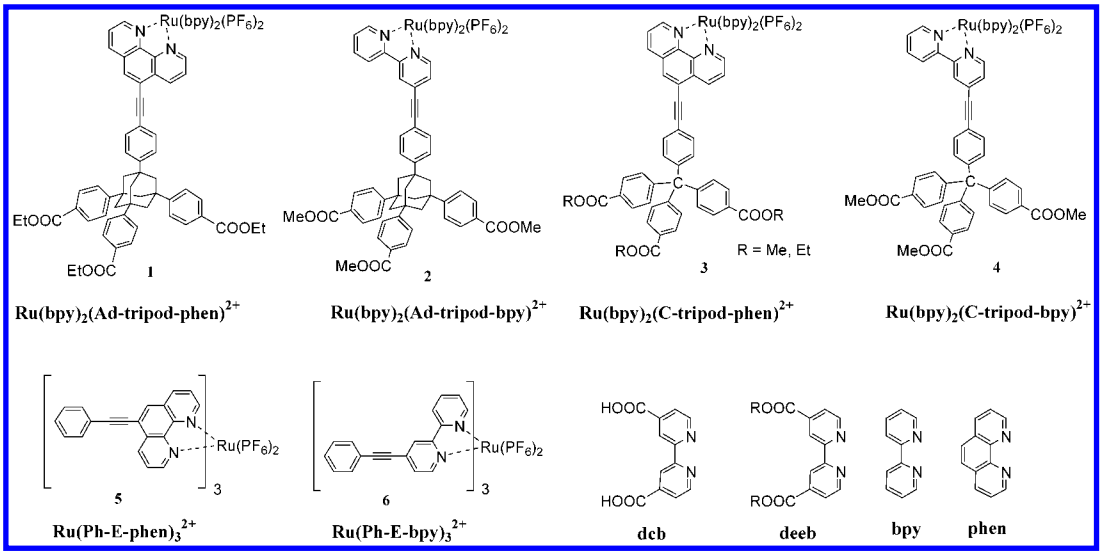

Figure 2. Structure of tripodal sensitizers **1**−**4**, reference complexes **5** and **6**, and the ligands employed in this study. The distances (*d*) to the Ru center from the tripod footprint for **1**−**4** are $d_1 = 17.6$ Å, $d_2 = 17.3$ Å, $d_3 = 15.7$ Å, and $d_4 = 15.4$ Å, respectively.

Charge recombination to the Ru^{III} center, which is several orders of magnitude slower, regenerates the ground state and occurs with second-order kinetics.[4]

In the state-of-the-art solar cells, the MLCT excited state is typically localized on a dcb or a terpyridine ligand substituted with carboxylic acid groups.[5] Depending on the surface binding conditions, the carboxylic acid substituents can react with surface hydroxyl groups to form ester linkages.[6] Such bonds are thought to provide strong electronic coupling between the dye and the semiconductor and underlie the ultrafast electron injection rate constants that have been measured.[3] In principle, however, such injection rates are not needed for efficient solar energy conversion, and interfacial charge separation yields of unity are expected when the rate constants for injection are 3−4 orders of magnitude slower.[3] In fact, an optimal electronic interaction may exist wherein the quantum yield for charge injection is still unity, while charge recombination is further inhibited. This scenario would be expected to increase the power output of the regenerative solar cell.[3]

Recently, several studies have demonstrated that excited states remote from the semiconductor surface can efficiently inject electrons into TiO_2.[7,8] To study these weakly coupled systems, researchers have prepared bimetallic coordination compounds[7] and sensitizers with flexible alkyl chains bridging the binding groups and the bpy ligand.[8] The former approach is not readily amenable to systematic studies, and in the latter approach semiconductor−sensitizer distances cannot be fixed. Clearly, there exists a need for *rigid* linkers that can be modified to systematically regulate the sensitizer−nanoparticle electronic interaction. Organic linkers that have such properties were developed recently in our laboratories and are schematically shown in Figure 1b.[9] These are rigid "tripods",[10] having a tetrahedral core made of tetraphenylmethane or 1,3,5,7-tetraphenyladamantane, three COOR surface binding groups, and a rigid-rod arm carrying the sensitizer. This design provides a stable, three-point attachment to the surface of metal oxide nanoparticles and a well-defined position of photoactive and/or redox-active groups on nanoparticle surfaces. The kinetic rate constants for remote interfacial electron-transfer processes can be quantified spectroscopically after selective light excitation of the sensitizer.

We recently reported the study of the first tripodal sensitizer, $Ru(bpy)_2(Ad\text{-}tripod\text{-}phen)^{2+}$ (**1** in Figure 2), in solution and bound to TiO_2 thin films.[11] We observed rapid ($k_{cs} > 10^8\ s^{-1}$) interfacial electron transfer in $Ru(bpy)_2(Ad\text{-}tripod\text{-}phen)^{2+}/TiO_2$ and efficient conversion of light into electricity when this material was utilized as photoanode in regenerative solar cells. In this article, we report additional results with **1** and the synthesis and study of three new tripodal sensitizers, $Ru(bpy)_2(Ad\text{-}tripod\text{-}bpy)^{2+}$ (**2**), $Ru(bpy)_2(C\text{-}tripod\text{-}phen)^{2+}$ (**3**), and $Ru(bpy)_2(C\text{-}tripod\text{-}bpy)^{2+}$ (**4**), shown in Figure 2. All four have a phenyethynyl unit as the rigid spacer and bpy as the auxiliary ligands, but they differ in the ligand (bpy or phen) and tetrahedral core (adamantane or an sp^3-hybridized carbon). Two

(4) Kelly, C. A.; Thompson, D. W.; Farzad, F.; Stipkala, J. M.; Meyer, G. J. *Langmuir* **1999**, *15*, 7047.
(5) (a) Nazeeruddin, M. K.; Kay, A.; Rodicio, I.; Humphry-Baker, R.; Müller, E.; Liska, P.; Vlachopoulos, N.; Grätzel, M. *J. Am. Chem. Soc.* **1993**, *115*, 6382. (b) Nazeeruddin, M. K.; Péchy, P.; Renouard, T.; Zakeeruddin, S. M.; Humphry-Baker, R.; Comte, P.; Liska, P.; Cevey, L.; Costa, E.; Shklover, V.; Spiccia, L.; Deacon, G. B.; Kay, A.; Bignozzi, C. A.; Grätzel, M. *J. Am. Chem. Soc.* **2001**, *123*, 1613.
(6) (a) Umpathy, S.; Cartner, A. M.; Parker, A. W.; Hester, R. E. *J. Phys. Chem.* **1990**, *94*, 1357. (b) Meyer, T. J.; Meyer, G. J.; Pfenning, B.; Schoonover, J. R.; Timpson, C.; Wall, J. F.; Kobusch, C.; Chen, X.; Peek, B. M.; Wall, C. G.; Ou, W.; Erickson, B. W.; Bignozzi, C. A. *Inorg. Chem.* **1994**, *33*, 3952. (c) Argazzi, R.; Bignozzi, C. A.; Heimer, T. A.; Castellano, F. N.; Meyer, G. J. *Inorg. Chem.* **1994**, *33*, 5741. (d) Finnie, K. S.; Bartlett, J. R.; Woolfrey, J. L. *Langmuir* **1998**, *14*, 2744. (e) Qu, P.; Meyer, G. J. *Langmuir* **2001**, *17*, 6720.
(7) (a) Argazzi, R.; Bignozzi, C.; Heimer, T. A.; Castellano, F. N.; Meyer, G. J. *Inorg. Chem.* **1994**, *33*, 5741. (b) Kleverlaan, C. J.; Indelli, M. T.; Bignozzi, C. A.; Pavanin, L.; Scandola, F.; Hasselmann, G. M.; Meyer, G. J. *J. Am. Chem. Soc.* **2000**, *122*, 2840. (c) Kleverlaan, C. J.; Alebbi, M.; Argazzi, R.; Bignozzi, C. A.; Hasselmann, G. M.; Meyer, G. J. *Inorg. Chem.* **2000**, *39*, 1342.
(8) (a) Heimer, T. A.; D'Arcangelis, S. T.; Farzad, F.; Stipkala, J. M.; Meyer, G. J. *Inorg. Chem.* **1996**, *35*, 5319. (b) Asbury, J. B.; Hao, E.; Wang, Y.; Lian, T. *J. Phys. Chem. B* **2000**, *104*, 11957.
(9) Guo, W.; Galoppini, E.; Rydja G. I.; Pardi, G. *Tetrahedron Lett.* **2000**, *41*, 7419.
(10) Tripod-shaped linkers of various structure (also termed caltrops, ref 10c) have been previously reported in studies of redox-active molecules bound on gold electrodes: (a) Whitesell, J. K.; Chang, H. K. *Science* **1993**, *261*, 73. (b) Fox, M. A.; Whitesell, J. K.; McKerrow, A. J. *Langmuir* **1998**, *14*, 816. (c) Yao, Y.; Tour, J. M. *J. Org. Chem.* **1999**, *64*, 1968. (d) Hu, J.; Mattern, L. *J. Org. Chem.* **2000**, *65*, 2277. (e) Hirayama, D.; Takimiya, K.; Aso, Y.; Otsubo, T.; Hasobe, T.; Yamada, H.; Imahori, H.; Fukuzumi, S.; Sakata, Y. *J. Am. Chem. Soc.* **2002**, *124*, 532.
(11) Galoppini, E.; Guo, W.; Qu, P.; Meyer, G. J. *J. Am. Chem. Soc.* **2001**, *123*, 4342.

model Ru^{II} complexes, **5** and **6**, with phenylethynyl arms on the phen and bpy ligands, were prepared: $Ru(Ph\text{-}E\text{-}phen)_3^{2+}$ (**5**) served as a model for the phen-based tripods **1** and **3**, and $Ru(Ph\text{-}E\text{-}bpy)_3^{2+}$ (**6**) for the bpy-based tripods **2** and **4**. Reference complexes $Ru(phen)_3^{2+}$, $Ru(bpy)_2(phen)^{2+}$, $Ru(bpy)_3^{2+}$, and $Ru(bpy)_2(deeb)^{2+}$ were also prepared.

Experimental Section

Characterization Data. For detailed synthetic procedures and methods, see Supporting Information.

1-(Trimethylsilylethynylphenyl)-3,5,7-tris(4-iodophenyl)adamantane (8, Td = Ad, X = I). Characterization data for **8** have been previously reported.[9]

4-Trimethylsilylethynylphenyl-tris(4-bromophenyl)methane (8, Td = C, X = Br): mp 225 °C (DSC); ^{1}H NMR δ 7.37 (m, 8H), 7.07 (d, 2H, J = 8.0 Hz), 7.00 (d, 6H, J = 8.0 Hz), 0.235 (s, 9H, Si(CH_3)$_3$); ^{13}C NMR δ 145.66, 144.49, 132.39, 131.50, 131.01, 130.49, 121.40, 120.72, 104.39, 94.99, 63.89, −0.08 (Si(CH_3)$_3$). Anal. Calcd for $C_{30}H_{25}Br_3Si$: C, 55.15; H, 3.86; Br, 36.69; Si, 4.30. Found: C, 54.90; H, 3.72. The disubstituted product, bis(4-trimethylsilylethynylphenyl)-bis-(4-bromophenyl)methane, was also isolated as a white solid (540 mg, 26%).[16]

4-Trimethylsilylethynylphenyl-tris(4-carbomethoxyphenyl)-methane (10, Td = C, R = Me): mp 78−80 °C; ^{1}H NMR δ 7.93 (d, 6H, J = 8.5 Hz), 7.38 (d, 2H, J = 8.5 Hz), 7.28 (d, 6H, J = 8.5 Hz), 7.13 (d, 2H, J = 8.5 Hz), 3.90 (s, 9H, COOCH_3), 0.235 (s, 9H, Si-(CH_3)$_3$); ^{13}C NMR δ 166.63 (*C*OOCH$_3$), 150.22, 145.31, 131.63, 130.74, 130.56, 129.22, 128.42, 121.52, 104.32 (*C*≡CSi), 95.10 (C≡*C*Si), 65.34, 52.18 (COO*C*H$_3$), −0.14 (Si(CH_3)$_3$). Anal. Calcd for $C_{36}H_{34}O_6Si$: C, 73.19; H, 5.80. Found: C, 73.30; H, 5.75.

Trimethylsilylethynylphenyl-3,5,7-tris(4-carbomethoxylphenyl)-adamantane (10, Td = Ad, R = Me): ^{1}H NMR δ 8.60 (d, 2H, J = 5.0 Hz), 8.04 (d, 6H, J = 8.0 Hz), 7.56 (two doublets overlap, 8H), 7.50 (d, 2H, J = 8.0 Hz), 7.38 (d, 2H, J = 5.0 Hz), 3.92 (s, 9H), 2.21 and 2.20 (two overlapping s, 12H); ^{13}C NMR δ 166.83, 153.70, 149.85, 149.71, 132.02, 131.40, 129.80, 128.30, 125.48, 125.20, 125.04, 120.13, 93.75, 86.64, 52.07, 46.58, 39.55, 39.34. The characterization data for **10** (Td = Ad, R = Et) have been reported.[9]

4-Ethynylphenyl-tris(4-carbomethoxyphenyl)methane (11, Td = C, R = Me): mp 158−160 °C; ^{1}H NMR δ 7.94 (d, 6H, J = 8.5 Hz), 7.41 (d, 2H, J = 8.5 Hz), 7.29 (d, 6H, J = 8.5 Hz), 7.16 (d, 2H, J = 8.5 Hz), 3.90 (s, 9H, COOCH_3), 3.08 (s, 1H, C≡C*H*); ^{13}C NMR δ 166.56 (*C*OOCH$_3$), 150.15, 145.66, 131.78, 130.70, 130.61, 129.23, 128.41, 120.51, 82.96 (*C*≡CH), 77.83 (C≡*C*H), 65.32, 52.14 (COO*C*H$_3$). Anal. Calcd for $C_{33}H_{26}O_6$: C, 76.43; H, 5.05. Found: C, 74.85; H, 5.43.

1-(Ethynylphenyl)-3,5,7-tris(4-carbomethoxylphenyl)adamantane (11, Td = Ad, R = Me): ^{1}H NMR δ 8.03 (d, 6H, J = 8.5 Hz), 7.54 (d, 6H, J = 8.5 Hz), 7.49 (d, 2H, J = 8.0 Hz), 7.43 (d, 2H, J = 8.0 Hz), 3.91 (s, 9H, OCH_3), 3.06 (s, 1H, C≡C*H*), 2.19 and 2.18 (2s, 12H, adamantane); ^{13}C NMR δ 166.83, 153.74, 149.33, 132.23, 129.78, 128.25, 125.03, 120.13, 83.37, 52.07, 46.57, 39.53, 39.21 (one C of the ethyne overlaps with the solvent). **11, Td = Ad, R = Et:** ^{1}H NMR δ 8.04 (d, 6H, J = 8.5 Hz), 7.54 (d, 6H, J = 8.5 Hz), 7.49 (d, 2H, J = 8.0 Hz), 7.43 (d, 2H, J = 8.0 Hz), 4.37 (q, 6H, J = 7.0 Hz, OCH_2CH$_3$), 3.07 (s, 1H, C≡C*H*), 2.21 and 2.19 (2s, 12H, adamantane), 1.39 (t, 9H, J = 7.0 Hz, OCH$_2$CH_3); ^{13}C NMR δ 166.39, 153.65, 149.39, 132.27, 129.76, 128.51, 124.64 (2C), 120.16, 83.38 (*C*≡CH), 60.91, 46.62 (2C), 39.58, 39.25, 14.34 (C≡*C*H overlaps with the solvent).

Ad-tripod-phen (12a). The characterization data for this ligand have been previously reported.[9]

Ad-tripod-bpy (12b): ^{1}H NMR δ 8.70 (d, 1H, J = 4.0 Hz), 8.65 (d, 1H, J = 5.0 Hz), 8.54 (bs, 1H), 8.41 (d, 1H, J = 8.0 Hz), 8.04 (d, 6H, J = 8.5 Hz), 7.83 (m, 1H), 7.55 (m, 8H), 7.50 (d, 2H, J = 8.0 Hz), 7.38 (d, 1H, J = 5.0 Hz), 7.34 (m, 1H), 3.92 (s, 9H, OCH_3), 2.21 (s, 12H, adamantane); ^{13}C NMR δ 166.86, 156.12, 155.48, 153.72, 149.75, 149.15, 136.99, 132.40, 132.08, 129.80, 128.26, 125.19, 125.16, 125.05, 123.99, 123.14, 121.11, 120.30, 93.73, 87.05, 52.07, 46.56, 39.54, 39.32; HRMS (FAB) calcd for $C_{52}H_{45}N_2O_6$ (MH^+) 793.9392, found 793.9371.

C-Tripod-phen (12c): mp 148−150 °C; ^{1}H NMR δ 9.24 (dd, 1H, J = 4.5 Hz, J = 1.5 Hz), 9.20 (dd, 1H, J = 4.5 Hz, J = 1.5 Hz), 8.80 (dd, 1H, J = 8.5 Hz, J = 2.0 Hz), 8.24 (dd, 1H, J = 8.5 Hz, J = 2.0 Hz), 8.10 (s, 1H), 7.97 (d, 6H, J = 8.5 Hz), 7.73 (q, 1H, J = 8.5 Hz, J = 4.0 Hz), 7.65 (dd, 1H, J = 8.0 Hz, J = 4.0 Hz), 7.59 (d, 2H, J = 9.0 Hz), 7.33 (d, 6H, J = 8.5 Hz), 7.27 (d, 2H, J = 9.0 Hz), 3.91 (s, 9H, COOCH_3); ^{13}C NMR δ 166.55 (*C*OOCH$_3$), 150.91, 150.62, 150.12, 146.07, 145.90, 145.86, 135.79, 134.62, 131.43, 130.85, 130.70, 129.28, 128.47, 128.19, 127.96, 123.46, 123.34, 120.99, 119.71, 94.70, 86.40, 65.41, 52.15 (COO*C*H$_3$) (one carbon overlaps in the aromatic region); LRMS (FAB) *m/z* (relative intensity) 698 (52, M^+ + 1), 697 (100, M^+). Anal. Calcd for $C_{45}H_{32}N_2O_6$: C, 77.57; H, 4.63; N, 4.02. Found: C, 74.87; H, 4.62; N, 3.53.

C-Tripod-bpy (12d): mp 98−100 °C; ^{1}H NMR δ 8.69 (d, 1H, J = 4.0 Hz), 8.66 (d, 1H, J = 5.0 Hz), 8.52 (s, 1H), 8.41 (d, 1H, J = 7.5 Hz), 7.96 (d, 6H, J = 7.5 Hz), 7.83 (m, 1H), 7.49 (d, 2H, J = 7.5 Hz), 7.38 (d, 1H, J = 5.0 Hz), 7.31 (m, 7H), 7.23 (d, 2H, J = 7.5 Hz), 3.91 (s, 9H); ^{13}C NMR δ 166.52, 156.14, 155.40, 150.08, 149.14, 149.12, 146.03, 136.96, 132.13, 131.55, 130.76, 130.67, 129.24, 128.41, 125.17, 123.96, 123.06, 121.09, 120.63, 93.16, 87.58, 65.36, 52.12; LRMS (FAB) *m/z* (relative intensity) 674 (51, M^+ + 1), 673 (100, M^+).

Ru(bpy)$_2$(Ad-tripod-phen)(PF$_6$)$_2$ (1, Td = adamantane, L = phen, R = Et). The characterization data for **1** have been reported.[11] IR: 2206 cm^{-1} (C≡C), 1708 cm^{-1} (C═O).

Ru(bpy)$_2$(Ad-Tripod-bpy)(PF$_6$)$_2$ (2, Td = adamantane, L = bpy, R = Me): ^{1}H NMR (acetone-d_6) δ 8.93 (m, 2H), 8.83 (d, 4H, J = 8.5 Hz), 8.18−8.26 (m, 6H), 8.08 (m, 5H), 8.03 (d, 6H, J = 8.5 Hz), 7.80 (m, 8H), ~7.59−7.65 (m, 8H), 3.88 (s, 9H, OCH$_3$), 2.32 (s, 12H, adamantane); ^{13}C NMR (acetone-d_6) δ 167.15, 158.49, 158.07, 157.73, 155.62, 152.93, 152.65, 139.07, 133.49, 133.00, 130.30, 129.65, 129.06, 128.83, 126.94, 126.47, 125.44, 119.78, 98.88, 86.37, 52.25, 46.97, 40.61; HRMS (FAB) calcd for $C_{72}H_6F_6O_6N_6PRu$ (M − PF_6) 1351.3392, found 1351.3367; IR 2206 cm^{-1} (C≡C), 1715 cm^{-1} (C═O); Raman shift 2207 cm^{-1} (C≡C).

Ru(bpy)$_2$(C-tripod-phen)(PF$_6$)$_2$ (3, Td = C, L = phen, R = Me): decomposes without melting above 250 °C (DSC); ^{1}H NMR δ 8.89 (d, 1H, J = 8.0 Hz), 8.45 (m, 5H), 8.33 (s, 1H), 8.13 (d, 1H, J = 5.0 Hz), 8.08 (d, 1H, J = 5.0 Hz), 7.93 (m, 11H), 7.80 (m, 3H), 7.58 (d, 2H, J = 8.0 Hz), 7.54 (d, 1H, J = 5.0 Hz), 7.51 (d, 1H, J = 5.0 Hz), 7.45 (m, 2H), 7.30 (m, 10H), 3.88 (s, 9H, COOCH_3); ^{13}C NMR δ 166.56 (*C*OOCH$_3$), 156.63, 152.86, 151.70, 151.39, 150.03, 147.21, 146.76, 138.15, 136.35, 135.44, 131.74, 131.37, 131.97, 130.68, 130.20, 129.33, 128.49, 128.19, 127.99, 127.21, 127.01, 124.20, 122.25, 120.00, 97.81, 84.38, 65.46, 52.18 (COO*C*H$_3$) (one carbon overlaps in the aromatic region). Anal. Calcd for the neutral complex: C, 55.76; H, 3.46; N, 6.00. Found: C, 56.03; H, 3.46; N, 5.91. **3, Td = C, L = phen, R = Et:** ^{1}H NMR δ 8.89 (d, 1H, J = 8.0 Hz), 8.41 (m, 5H), 8.32 (s, 1H), 8.15 (d, 1H, J = 4.5 Hz), 8.09 (d, 1H, J = 4.5 Hz), 7.93 (m, 11H), 7.83 (m, 3H), 7.55 (m, 4H), 7.47 (m, 2H), 7.31 (m, 10H), 4.35 (q, 6H, J = 7.0 Hz), 1.36 (t, 9H, J = 7.0 Hz); ^{13}C NMR δ 166.08, 156.59, 152.98, 151.84, 151.53, 149.95, 147.20, 146.75, 138.12, 137.96, 136.28, 135.45, 131.70, 131.29, 131.00, 130.65, 130.18, 129.30, 128.86, 128.27, 128.03, 127.26, 127.10, 124.09, 122.33, 119.92,

(12) Wilson, L. M.; Griffin A. C. *J. Mater. Chem.* **1993**, *3*, 991.
(13) Eichert, V. R.; Mathias, L. J. *Macromolecules* **1994**, *27*, 7015.
(14) Mizuno, T.; Masayuki, M.; Hamachi, I.; Nakashima, K.; Shinkai, S. *J. Chem. Soc., Perkin Trans. 2* **1998**, 2281.
(15) Hissler, M.; Connick, W. B.; Geiger, D. K.; McGarrah, J. E.; Lipa, D.; Lachicotte, R. J.; Eisenberg, R. *Inorg. Chem.* **2000**, *39*, 447.
(16) The di- and trisubstituted byproducts obtained in this step were isolated and characterized. Their syntheses and the study of di- and trichromophoric compounds prepared from them will be published elsewhere.

97.93, 84.29, 65.47, 61.07, 14.31; IR 2208 cm^{-1} (C≡C), 1716 cm^{-1} (C═O); Raman shift 2204 cm^{-1} (C≡C). Anal. Calcd for the neutral complex: C, 56.63; H, 3.77; N, 5.83. Found: C, 56.46; H, 3.71; N, 5.76.

$Ru(bpy)_2$(C-tripod-bpy)$(PF_6)_2$ (4, Td = C, L= bpy, R = Me): mp 224 °C (DSC); ^{1}H NMR (acetone-d_6) δ 8.91 (m, 2H), 8.83 (d, 4H, J = 8.0 Hz), 8.23 (m, 5H), 8.18 (d, 1H, J = 5.5 Hz), 8.08 (d, 2H, J = 6.0 Hz), 8.05 (d, 3H, J = 5.5 Hz) 7.97 (d, 6H, J = 8.5 Hz), 7.60 (m, 8H), 7.45 (d, 6H, J = 8.5 Hz), 7.41 (d, 2H, J = 8.5 Hz), 3.88 (s, 9H); ^{13}C NMR (acetone-d_6) δ 166.77, 158.47, 157.99, 157.97, 157.95, 157.90, 157.59, 152.76, 152.67, 152.53, 151.12, 148.33, 139.00, 133.06, 132.64, 131.96, 131.63, 129.98, 129.65, 129.35, 128.99, 128.75, 126.87, 126.69, 125.53, 125.39, 125.29, 125.19, 120.37, 97.92, 86.87, 66.38, 52.39; IR 2208 cm^{-1} (C≡C), 1716 cm^{-1} (C═O); Raman shift 2204 cm^{-1} (C≡C). Anal. Calcd for the neutral complex: C, 54.99; H, 3.52; N, 6.11. Found: C, 54.10; H, 3.75; N, 6.01.

Ph-E-phen (13):[17] mp 149−150 °C; ^{1}H NMR δ 9.24 (d, 1H, J = 4.5 Hz), 9.20 (d, 1H, J = 4.5 Hz), 8.85 (d, 1H, J = 8.5 Hz), 8.24 (d, 1H, J = 8.5 Hz), 8.11 (s, 1H), 7.75 (q, 1H, J = 4.5 Hz), 7.68 (m, 3H), 7.44 (m, 3H); ^{13}C NMR δ 150.83, 150.59, 146.05, 145.88, 135.72, 134.67, 131.71, 130.55, 128.92, 128.52, 128.22, 127.98, 123.40, 123.31, 122.52, 119.90, 95.33, 85.76.

Ru(Ph-E-phen)$(PF_6)_2$ (5): mp 255 °C (DSC); ^{1}H NMR (acetonitrile-d_3) δ 9.02 (d, 1H, J = 8.0 Hz), 8.58 (d, 1H, J = 8.0 Hz), 8.50 (s, 1H), 8.08 (m, 2H), 7.77 (m, 2H), 7.72 (m, 1H), 7.64 (m, 1H), 7.52 (m, 3H); ^{13}C NMR (acetonitrile-d_3) δ 154.56, 148.96, 148.64, 137.54, 136.57, 136.35, 132.91, 132.51, 132.31, 131.71, 131.50, 130.89, 129.90, 127.28, 122.61, 122.59, 98.40, 84.91. Anal. Calcd for the neutral complex: C, 58.50; H, 2.95; N, 6.82. Found: C, 57.53; H, 2.80; N, 6.80.

Ph-E-bpy (14): mp 90−92 °C; ^{1}H NMR δ 8.71 (d, 1H, J = 4.0 Hz), 8.67 (d, 1H, J = 5.0 Hz), 8.54 (s, 1H), 8.41 (d, 1H, J = 8.0 Hz), 7.84 (t, d, 1H, J = 8.0 Hz, J = 2.0 Hz), 7.57 (m, 2H), 7.39 (m, 4H), 7.34 (m, 1H); ^{13}C NMR δ 156.16, 155.52, 149.19, 149.14, 136.97, 132.42, 131.88, 129.10, 128.45, 125.22, 123.96, 123.15, 122.21, 121.12, 93.89, 87.01.

Ru(Ph-E-bpy)$(PF_6)_2$ (6): mp 209 °C (DSC); ^{1}H NMR δ 8.97 (m, 2H), 8.28 (m, 1H), 8.24 (m, 1H), 8.11 (m, 1H), 7.64 (m, 4H), 7.53 (m, 3H); ^{13}C NMR δ 158.45, 158.36, 157.64, 157.55, 152.86, 152.80, 139.26, 133.59, 132.86, 131.19, 129.85, 129.19, 127.11, 122.03, 98.68, 86.40. Anal. Calcd for the neutral complex: C, 55.92; H, 3.13; N, 7.25. Found: C, 55.31; H, 3.05; N, 7.20.

MO_2 Preparations. Transparent thin films of TiO_2 or ZrO_2 were prepared by a modification of published procedures[18] that is described in the Supporting Information.

Spectroscopic Measurements. UV−vis absorbance measurements were made on a Hewlett-Packard 8453 diode array spectrophotometer. For TiO_2 and ZrO_2 studies, transient absorption measurements were acquired using 532.5 nm laser excitation, ca. 8 ns and 1−20 mJ cm^{-2}, from a Nd:YAG (Continuum Surelite II) laser. For transient absorption experiments in fluid acetonitrile solution, samples were excited with 417 nm (Raman-shifted 355 nm laser light using a D_2-filled pressurized tube). The 5 mm diameter beam was expanded to ensure homogeneous irradiation of the entire film. The sample was protected from a pulsed 150 W Xe probe beam using a fast shutter and appropriate UV- and heat-absorbing glass and solution filter combinations. Each kinetic trace was acquired by averaging 10−160 laser shots (typically 40). Samples were argon purged and maintained under an acetonitrile premoistened argon flow.

Infrared and Raman. Attenuated total reflectance (ATR) IR measurements for solid samples of **1**−**4** were made on a Bruker Vector 22 spectrometer using a Pike Miracle ATR accessory with 2 cm^{-1} resolution and 64 or 256 scans. IR measurements of the tripods on TiO_2 were made in transmission mode with unsensitized, pH 1 pretreated TiO_2/sapphire as the reference. Raman spectra of solid samples of **1**−**4** were collected on a Thermo-Nicolet Nexus 670 FT-Raman Module.

Photoluminescence. Corrected photoluminescence (PL) spectra were obtained with a Spex Fluorolog that had been calibrated with a standard tungsten−halogen lamp using procedures provided by the manufacturer. Sensitized films were placed diagonally in a 1 cm square cuvette, immersed in acetonitrile, and argon purged for at least 15 min. The excitation beam was directed 45° to the film surface, and the emitted light was monitored from the front face of the surface-bound sample and from the right angle in the case of fluid solutions. Photoluminescence quantum yield measurements were performed using the optically dilute technique[19] with $Ru(bpy)_3Cl_2$ in deionized H_2O as the actinometer, and calculated using eq 1,

$$\phi_{em} = (A_r/A_s)(I_s/I_r)(n_s/n_r)^2\phi_r \quad (1)$$

where A_r and A_s are the absorbances of the actinometer and sample, respectively, I_r and I_s are the integrated photoluminescences of the actinometer and sample, respectively, n_r and n_s are the refraction indexes for the solvents used for the actinometer and sample, respectively, and ϕ_r is the quantum yield for $Ru(bpy)_3Cl_2$ in deionized H_2O (ϕ_r = 0.042).

Time-Resolved Photoluminescence. Time-resolved photoluminescence decays were acquired on a nitrogen-pumped dye laser (460 nm) apparatus that has been previously described.[20] For solution studies, the samples were optically dilute ($A \approx 0.1$ at λ_{max}), and the kinetic traces were fit to a first-order model. Values for k_r and k_{nr} were calculated from eqs 2a and 2b

$$\phi_{em} = k_r/(k_r + k_{nr}) \quad (2a)$$

$$\phi_{em} = k_r\tau \quad (2b)$$

using the measured quantum yields and lifetimes and assuming an intersystem crossing yield of unity. For studies involving the tripods on TiO_2 or ZrO_2, the excitation beam was directed 45° to the film surface, and the emitted light was collected at 90°.

Electrochemistry. Cyclic voltammetry for solution studies was performed in 0.1 M tetrabutylammonium hexafluorophosphate ($TBAPF_6$)/CH_3CN electrolyte. The solutions were ~1 mM in the dyes. A BAS model CV-50W potentiostat was used in a standard three-electrode arrangement consisting of a glassy carbon working electrode, a Pt gauze counter electrode, and Ag/AgCl as the reference electrode. Cyclic voltammetry of the sensitizers bound to TiO_2 was performed in a similar manner with the sensitizer/TiO_2 films deposited on FTO glass as the working electrodes submerged in 0.1 M tetrabutylammonium perchlorate ($TBAClO_4$) acetonitrile (see Figure S1, Supporting Information). The CV experiments were carried out under argon atmosphere and at room temperature.

Spectroelectrochemistry. Solution measurements were carried out in a 1 mm path-length quartz cuvette consisting of a Pt wire reference electrode and a Pt gauze working electrode. The counter electrode consisted of a glass cell containing a Pt wire in $TBAClO_4/CH_3CN$ electrolyte separated from the sensitizer solution by a glass frit. A PAR 173 potentiostat was used to control the applied potential, and a Hewlett-Packard 8453 diode array was used to monitor the absorbance changes at different applied potentials. The concentration of all solutions was adjusted to obtain less than 0.1 absorbance unit at λ_{max}.

Spectroelectrochemistry of derivatized TiO_2 (pH 1 pretreated) electrodes was performed in a three-electrode cell compartment using

(17) The synthesis of Ph-E-phen through a different route has been reported: McGarrah, J. E.; Kim, Y.-I.; Hissler, M.; Eisenberg, R. *Inorg. Chem.* **2001**, *40*, 4510.
(18) O'Regan, B.; Moser, J.; Anderson, M.; Grätzel, M. *J. Phys. Chem*. **1990**, *94*, 8720.
(19) Demas, J. N.; Crosby, G. A. *J. Phys. Chem*. **1971**, *75*, 991.
(20) Castellano, F. N.; Heimer, T. A.; Tandhasetti, T.; Meyer, G. J. *Chem. Mater*. **1994**, *6*, 1041.

Scheme 1 [a]

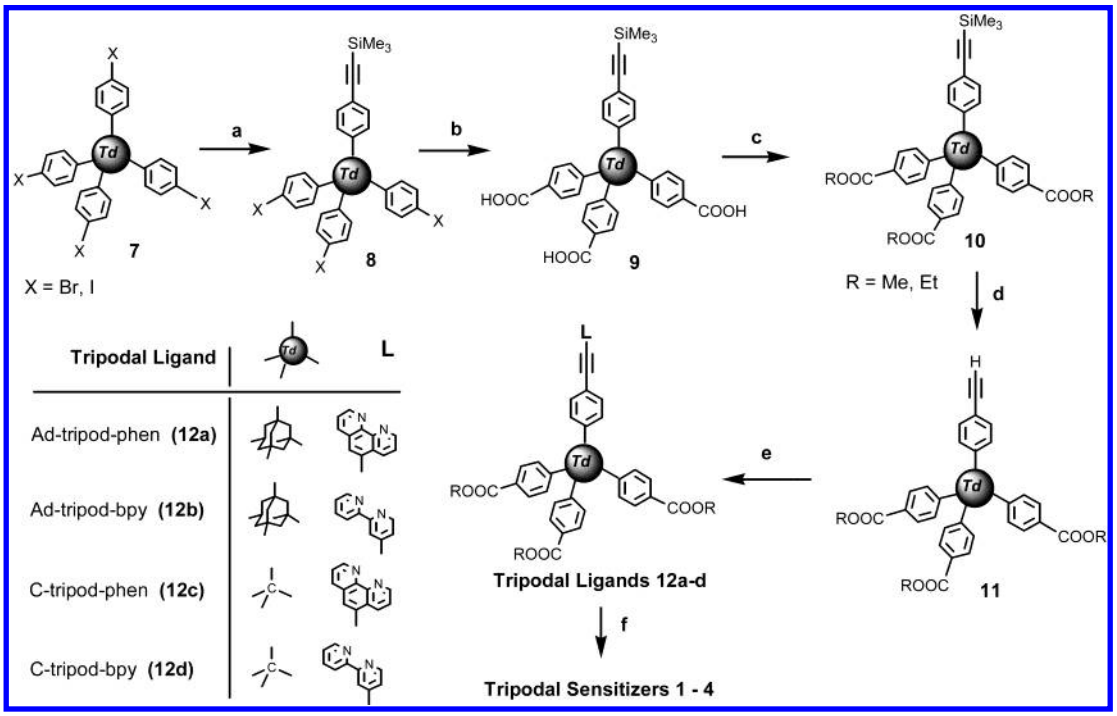

[a] Reagents and yields: (a) $Me_3SiC{\equiv}H$ (1.5 equiv), $Cl_2Pd(PPh_3)_2$, CuBr, $(i\text{-}Pr)_2NH$ (22−30%); (b) 1. *t*-BuLi; 2. CO_2; 3. H^+, H_2O (50%); (c) CH_2N_2 (90%) (R = Me) or dicyclohexylcarbodiimide and EtOH (R = Et); (d) *n*-Bu_4NF (95%); (e) 1. $(Me_3Si)_2NLi$; 2. B-methoxy-9-BBN, 4-bromo-2,2′-bipyridine, or 5-bromo-1,10-phenanthroline, $Pd(PPh_3)_4$ (36−68%); (f) 1. $Ru(bpy)_2Cl_2{\cdot}2H_2O$; 2. NH_4PF_6 (55−75%).

a sensitizer/TiO_2 film deposited on FTO glass as the working electrode, Pt gauze as the counter electrode, and Ag/AgCl as the reference electrode in 0.1 M $TBAClO_4/CH_3CN$. Oxidative chronoabsorptometry measurements were performed on derivatized TiO_2 electrodes by stepping the potential from 1.2 to 1.65 V and taking spectra every 5 s. Reductive chronoabsorptometry measurements were performed by stepping the potential from 1.65 to 1.0 V and taking spectra every 5 s.

Results

Synthesis. Tripodal sensitizers **1**−**4** were prepared as shown in Scheme 1. Monosubstituted **8** was obtained by Sonogashira cross-coupling[21] of trimethylsilylacetylene with the tetrabromide or tetraiodide derivative of tetraphenylmethane[12] or 1,3,5,7-tetraphenyladamantane,[13] respectively. Carboxylation of **8** followed by esterification of the acid, **9**,[22] afforded trimethylsilylethyne **10**,[16] which was deprotected with fluoride to form alkyne **11**. Suzuki-type coupling[23] of **11** with 5-bromo-1,10-phenanthroline or 4-bromo-2,2′-bipyridine produced the series of four tripodal ligands Ad-tripod-phen (**12a**), Ad-tripod-bpy (**12b**), C-tripod-phen (**12c**), and C-tripod-bpy (**12d**), all solid materials that were soluble in polar organic solvents.

The corresponding Ru^{II}-polypyridyl complexes **1**−**4** were prepared upon treatment with $Ru(bpy)_2Cl_2{\cdot}2H_2O$ and precipitation with NH_4PF_6. Similar procedures were used to prepare model complexes **5** and **6** from lithium phenylacetylide (Scheme 2).

Binding Constants. Surface binding was monitored spectroscopically by measuring the change in film and solution absorbance after soaking the film for 12 h in acetonitrile solutions with known concentrations of the tripodal sensitizer. In all cases, the surface coverage saturated at high sensitizer concentration. The equilibrium binding for **1**−**4** was well described by the Langmuir adsorption isotherm model from which surface adduct formation constants (K_{ad}) were abstracted using eq 3,[24] where $[Ru^{II}]_{eq}$ is the equilibrium sensitizer

$$\frac{[Ru^{II}]_{eq}}{\Gamma} = \frac{1}{K_{ad}\Gamma_0} + \frac{[Ru^{II}]_{eq}}{\Gamma_0} \qquad (3)$$

concentration, Γ_0 is the saturation coverage, and Γ is the equilibrium coverage at a defined molar concentration. The plots of $[Ru^{II}]_{eq}/\Gamma$ versus $[Ru^{II}]_{eq}$ for **1**−**4** are shown in Figure 3, insets. The surface adduct formation constants ($\sim 10 \times 10^5\ M^{-1}$, Table 3) are approximately 1 order of magnitude larger than those of Ru^{II}-polypyridyl complexes attached to untreated metal oxides surfaces via dcb or deeb ligands. The typical equilibrium surface coverage for **1**−**4** is $(3 \pm 2) \times 10^{-8}$ mol cm^{-2},

Scheme 2 [a]

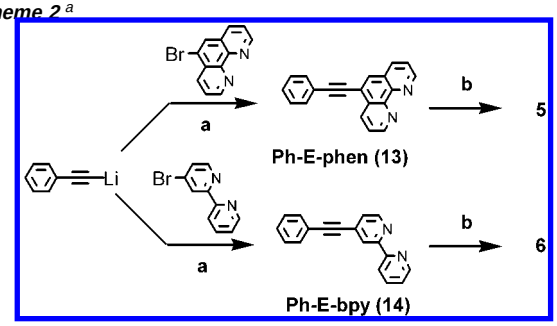

[a] Reagents and yields: (a) 1. B-methoxy-9-BBN; 2. $Pd(PPh_3)_4$ (90%); (b) 1. $RuCl_3{\cdot}2H_2O$; 2. $NaPF_6$ (69%).

(21) Sonogashira, K. In *Comprehensive Organic Synthesis*; Trost, B. M., Ed.; Pergamon Press: Oxford, 1991; Vol. III, p 551.
(22) While the acids are insoluble materials, the esters are soluble in organic solvents and can be purified by column chromatography. Ethyl esters were more soluble than methyl esters, but the latter were obtained in considerably higher yields.
(23) (a) Soderquist, T. A.; Matos, K.; Rane, A.; Ramos, J. *Tetrahedron Lett.* **1995**, *36*, 2401. (b) Miyaura, N.; Suzuki, A. *Chem. Rev.* **1995**, *95*, 2457.
(24) Langmuir, I. *J. Am. Chem. Soc.* **1918**, *40*, 1361.

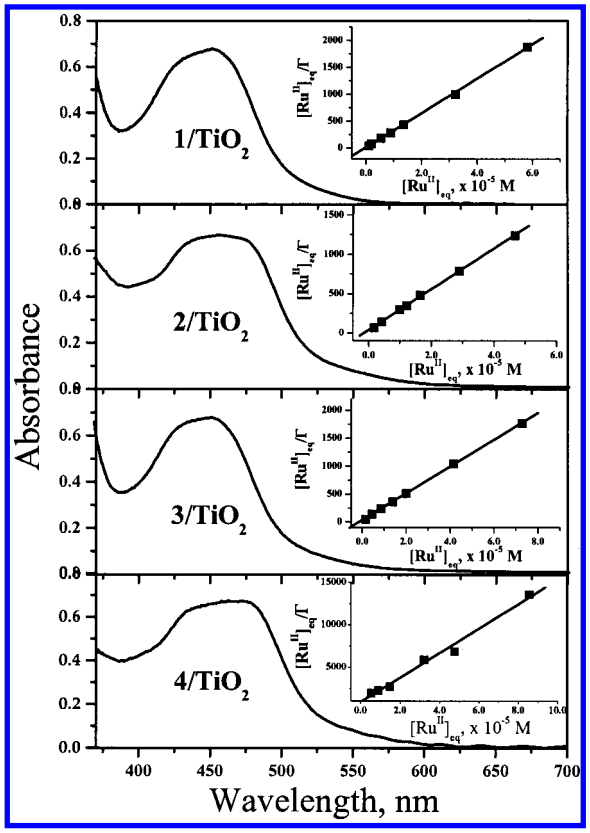

Figure 3. Absorption spectra of **1**−**4** bound to TiO_2 films and immersed in CH_3CN. Insets: Plots of $[Ru^{II}]_{eq}/\Gamma$ vs $[Ru^{II}]_{eq}$ with overlaid linear fits.

comparable to that obtained from Ru^{II}-polypyridyl complexes that are directly attached to the surface through a dcb or deeb ligand ($(5 \pm 4) \times 10^{-8}$ mol cm^{-2}).

Solution and Surface-Bound Electrochemistry. The tripodal sensitizers displayed quasi-reversible[25a] $Ru^{III/II}$ waves in acetonitrile solution at 1.32 V vs SCE (Table 1). The $Ru^{III/II}$ reduction potentials for phen- as well as bpy-based tripods were 60−90 mV more positive than those observed for $Ru(bpy)_2(phen)^{2+}$ and $Ru(bpy)_3^{2+}$. Similarly, the $Ru^{III/II}$ reduction potentials for model complexes $Ru(Ph\text{-}E\text{-}phen)_3^{2+}$ and $Ru(Ph\text{-}E\text{-}bpy)_3^{2}$ were 100 and 170 mV more positive than those observed for $Ru(phen)_3^{2+}$ and $Ru(bpy)_3^{2+}$, respectively.

Ligand-based reduction potentials for the tripodal sensitizers in solution are shown in Table 2. The first ligand reductions for **1**−**4** occur at potentials that are more positive (∼85−100 mV) than those observed for the other Ru^{II}-polypyridyl complexes listed. Similarly, in model complexes $Ru(Ph\text{-}E\text{-}phen)_3^{2+}$ (**5**) and $Ru(Ph\text{-}E\text{-}bpy)_3^{2+}$ (**6**), a ligand is first reduced at a potential that is 230 and 180 mV more positive than those observed for $Ru(phen)_3^{2+}$ and $Ru(bpy)_3^{2+}$, respectively. Therefore, we assigned this wave in **1**−**6** to the phen or bpy ligand connected to the phenylethynyl spacer.[26] Single cathodic prepeaks were observed for **1**−**6** at ∼ −850 mV on the initial scans but were absent after multiple scans. Furthermore, the reoxidation wave corresponding to the second ligand reduction appears as a sharp anodic peak for **1**−**6**, which is characteristic of anodic desorption of the neutral species from the glassy carbon surface.[25]

Cyclic voltammetry performed on derivatized TiO_2 films (Table 3) showed reversible oxidation of the Ru^{II} center and $Ru^{III/II}$ potentials that did not significantly deviate from values obtained in fluid solution. The electroactive surface coverage, estimated by integration of the anodic or cathodic waves at scan rates of 20−200 mV/s, like that shown in Figure S1 (Supporting Information), was a fraction of that measured spectroscopically, consistent with previous observations reported by us[11] and by others.[27] Complete oxidation of all the surface-bound complexes was accomplished by stepping the potential positive of $E_{1/2}(Ru^{III/II})$ for about 1 h, *vide infra*.

The excited-state reduction potentials were calculated from the ground-state potentials and the free energy stored in the thermally equilibrated MLCT excited state, ΔG_{es}, using eq 4. ΔG_{es} (in eV) was estimated by drawing a tangent line to the

$$E_{1/2}(Ru^{III/II*}) = E_{1/2}(Ru^{III/II}) - \Delta G_{es} \qquad (4)$$

high-energy side of the corrected emission spectra. $Ru(bpy)_2(Ad\text{-}tripod\text{-}phen)^{2+}$ and $Ru(bpy)_2(C\text{-}tripod\text{-}phen)^{2+}$ had identical excited-state reduction potentials (−910 mV), and those of $Ru(bpy)_2(Ad\text{-}tripod\text{-}bpy)^{2+}$ and $Ru(bpy)_2(C\text{-}tripod\text{-}bpy)^{2+}$ (∼−815 mV) were also the same within experimental error. The excited-state reduction potentials for phen-based tripodal sensitizers **1** and **3** were the same as that observed for phen-based model complex **5**, $Ru(Ph\text{-}E\text{-}phen)_3^{2+}$, and the excited-state reduction potentials for bpy-based tripodal sensitizers **2** and **4** were about the same as that observed for bpy-based model complex **6**, $Ru(Ph\text{-}E\text{-}bpy)_3^{2+}$. For the model complexes **5** and **6**, the potentials were ∼60 mV more positive than those for $Ru(phen)_3^{2+}$ and $Ru(bpy)_3^{2+}$, respectively.

Chronoabsorptometry measurements were performed on the tripods and $Ru(bpy)_2(deeb)^{2+}$ anchored to pH 1 pretreated TiO_2 films on FTO electrodes. Apparent diffusion coefficients (D_{app}) were obtained from linear fits of absorption changes versus $t^{1/2}$ according to the Cottrell equation, eq 5,

$$\Delta A = (2A_{max}D_{app}{}^{1/2}t^{1/2})/(d\pi^{1/2}) \qquad (5)$$

where ΔA is the change in absorbance at time t, A_{max} is the absorbance at which absorbance changes cease, D_{app} is the apparent diffusion coefficient in cm^2/s, and d is the thickness of the film in cm. Plots of ΔA versus $t^{1/2}$ maintained linearity for ∼70% of either the oxidative ($Ru^{II} \rightarrow Ru^{III}$) or reductive ($Ru^{III} \rightarrow Ru^{II}$) process. For both the tripods and $Ru(bpy)_2(deeb)^{2+}$, values for D_{app} for either the oxidative or reductive process were $\sim 10^{-11}$ cm^2/s.

Solution and Surface-Bound Photophysics. The visible absorption spectra of tripodal sensitizers **1**−**4** displayed broad bands typical of MLCT excited states (Figure S2, Supporting Information). The phen-based tripods, $Ru(bpy)_2(Ad\text{-}tripod$-

(25) (a) Bard, A. J.; Faulkner, L. R. *Electrochemical Methods: Fundamentals and Applications*; Wiley-Interscience: New York, 1980. (b) Del Guerzo, A.; Leroy, S.; Fages, F.; Schmehl, R. H. *Inorg. Chem.* **2002**, *41*, 359.

(26) For a similar example, where electron-withdrawing substituents in Ru^{II} complexes lead to a more positive shift in a ligand reduction wave, see: (a) Albano, G.; Belser, P.; De Cola, L.; Gandolfi, M. T. *Chem. Commun.* **1999**, 1171. (b) Kalyanasundarum, K. *Coord. Chem. Rev.* **1982**, *46*, 159. (c) Juris, A.; Balzani, V.; Barigelletti, F.; Belser, P.; Von Zelewsky; A. *Coord. Chem. Rev.* **1988**, *84*, 85.

(27) (a) Heimer, T. A.; D'Arcangelis, S. T.; Farzad, F.; Stipkala, J. M.; Meyer, G. J. *Inorg. Chem.* **1996**, *35*, 5319. (b) Bonhote, P.; Gogniat, E.; Tingry, S.; Barbe, C.; Vlachopoulos, N.; Lenzmann, F.; Comte, P.; Grätzel, M. *J. Phys. Chem. B* **1998**, *102*, 1498. (c) Farzad, F. Molecular Level Energy and Electron Transfer Processes at Nanocrystalline Titanium Dioxide Interfaces. Ph.D. Thesis, Johns Hopkins University, 1999. (d) Trammell, S. A.; Meyer, T. J. *J. Phys. Chem. B* **1999**, *103*, 104.

Table 1. Electrochemical and Photophysical Properties of **1**−**6** and Other Ru^{II}-Polypyridyl Sensitizers in Solution

sensitizer	λ_{abs}, nm[a] (ϵ, M^{-1} cm^{-1})	λ_{PL}[b] (nm)	τ[c] (μs)	$E_{1/2}(Ru^{III/II})$[d] (V)	$E_{1/2}(Ru^{III/II*})$ (V)	Φ_{PL} ($\times10^{-2}$)	k_r ($\times10^4$ s^{-1})	k_{nr} ($\times10^5$ s^{-1})	ΔG_{es} (eV)	ν(C═O)[e] (cm^{-1})
$Ru(bpy)_2(Ad\text{-}tripod\text{-}phen)^{2+}$ (**1**)	452 (1.6×10^4)	624	1.4	1.32	−0.91	8.0	5.7	6.6	2.23	1709
$Ru(bpy)_2(Ad\text{-}tripod\text{-}bpy)^{2+}$ (**2**)	461 (1.9×10^4)	646	2.0	1.32	−0.82	10	5.1	4.5	2.14	1715
$Ru(bpy)_2(C\text{-}tripod\text{-}phen)^{2+}$ (**3**)	450 (1.7×10^4)	626	1.0	1.32	−0.91	7.9	7.9	9.2	2.23	1716
$Ru(bpy)_2(C\text{-}tripod\text{-}bpy)^{2+}$ (**4**)	461 (2.0×10^4)	650	2.2	1.32	−0.81	10	4.8	4.1	2.13	1716
$Ru(Ph\text{-}E\text{-}phen)_3^{2+}$ (**5**)	449	605	1.1	1.37	−0.88	6.4	6.1	8.9	2.25	
$Ru(Ph\text{-}E\text{-}bpy)_3^{2+}$ (**6**)	468	605	1.1	1.43	−0.82	13	13	8.2	2.25	
$Ru(bpy)_2(phen)^{2+}$	450	620	1.2	1.23	−0.91				2.14	
$Ru(bpy)_3^{2+}$[f]	452	626	0.80	1.26	−0.86				2.12	
$Ru(phen)_3^{2+}$[f,g]	447	- -	0.30	1.27	−0.92				2.19	
$Ru(bpy)_2(deeb)^{2+}$[h]	475 (1.6×10^4)	690	0.93	1.39	−0.62	4.4	4.8	10	2.01	1732

[a] Measurement were made at 22 ± 2 °C, absorption maximum ±2 nm. The molar extinction coefficients, ϵ, were obtained from CH_3CN solutions. A TiO_2 film was used as the optical reference. [b] Photoluminescence maximum, ±4 nm. All data were obtained from CH_3CN solutions under an argon atmosphere. [c] Excited-state lifetime ±5%. Data were obtained from CH_3CN solutions. [d] Half-wave potentials (±20 mV) were measured at a glassy carbon working electrode in 0.1 M $TBAPF_6/CH_3CN$ solution using Ag/AgCl as reference. Data are reported vs SCE. [e] IR-ATR was performed on solid samples. [f] These complexes have unsubstituted phen and bpy as the ligands and cannot be bound to metal oxide surfaces. [g] Reference 39. [h] Reference 4.

Table 2. Electrochemical Data for **1**−**6** and Other Ru^{II}-Polypyridyl Sensitizers in Solution[a]

sensitizer	$E_{1/2}(Ru^{III/II})$ (mV)	$E_{1/2}(Ru^{2+/+})$ (mV)	$E_{1/2}(Ru^{+/0})$ (mV)	$E_{1/2}(Ru^{III/II}*)$ (mV)
$Ru(bpy)_2(Ad\text{-}tripod\text{-}phen)^{2+}$	1320	−1306	−1477	−910
$Ru(bpy)_2(Ad\text{-}tripod\text{-}bpy)^{2+}$	1320	−1246	−1485	−820
$Ru(bpy)_2(C\text{-}tripod\text{-}phen)^{2+}$	1320	−1270	−1463	−910
$Ru(bpy)_2(C\text{-}tripod\text{-}bpy)^{2+}$	1320	−1237	−1497	−810
$Ru(Ph\text{-}E\text{-}bpy)_3^{2+}$	1430	−1159	−1321	−820
$Ru(Ph\text{-}E\text{-}phen)_3^{2+}$	1370	−1140	−1301	−880
$Ru(bpy)_3^{2+}$	1260[b]	−1340[c]	−1520[c]	−860[b]
$Ru(phen)_3^{2+}$	1270[b]	−1370[c]	−1520[c]	−920[b]
$Ru(bpy)_2(phen)^{2+}$	1230[b]	−1370[c]	−1530[c]	−910[b]
$Ru(bpy)_2(4,7\text{-}dpphen)^{2+}$	1240[b]	−1320[c]		−870[b]
$Ru(bpy)_2(4,4'\text{-}dpbpy)^{2+}$	1230[b]	−1310[c]		−870[b]
$Ru(4,4'\text{-}dpbpy)_3^{2+}$	1190[d]	−1270[d]		

[a] Data are reported vs SCE. All measurements were performed in 0.1 M $TBAPF_6/CH_3CN$. Data obtained from the literature were performed in 0.1 M $TAAX/CH_3CN$, where $X = ClO_4^-$ or PF_6^- and $TAA = (N(Et)_4)^+$ or $(N(^nBu)_4)^+$. $E_{1/2}(Ru^{2+/+})$ and $E_{1/2}(Ru^{+/0})$ are the midpoint potentials for the first and second ligand reductions, respectively. [b] Reference 39. [c] Reference 40. [d] Reference 41. (V)

Table 3. Electrochemical, Adsorption, and IR Properties of **1**−**4** Bound to TiO_2

sensitizer	$E_{1/2}(Ru^{III/II})$[a] (V)	binding constant K_{ad}[b] ($\times10^5$ M^{-1})	surface coverage[c] ($\times10^{-8}$ mol cm^{-2})	ν(C═O)[d] (cm^{-1})
$Ru(bpy)_2(Ad\text{-}Tripod\text{-}phen)^{2+}$	1.34	30 ± 20	3.1	1720
$Ru(bpy)_2(Ad\text{-}Tripod\text{-}bpy)^{2+}$	1.35	10 ± 5	3.9	1718
$Ru(bpy)_2(C\text{-}Tripod\text{-}phen)^{2+}$	1.37	10 ± 5	4.2	1717
$Ru(bpy)_2(C\text{-}Tripod\text{-}bpy)^{2+}$	1.34	10 ± 5	2.0	1718

[a] Half-wave potentials (±20 mV) were measured at a sensitizer/TiO_2/FTO working electrode in 0.1 M $TBAClO_4/CH_3CN$ solution using Ag/AgCl as reference. Data are reported vs SCE. [b] Estimated from Langmuir adsorption isotherm measurements at 22 ± 2 °C. [c] From Langmuir adsorption isotherm measurements. [d] Obtained for samples of sensitizer/TiO_2/sapphire in the transmission mode.

phen)$^{2+}$ and $Ru(bpy)_2(C\text{-}tripod\text{-}phen)^{2+}$, displayed MLCT bands centered at ~451 nm, while the bpy-based tripods, $Ru(bpy)_2(Ad\text{-}tripod\text{-}bpy)^{2+}$ and $Ru(bpy)_2(C\text{-}tripod\text{-}bpy)^{2+}$, were red-shifted and centered at 461 nm. All complexes displayed room-temperature photoluminescence (PL) in fluid solution, and the emission maximum followed the same trends as the absorption (Table 1). Absorption and emission spectra of **1**−**4** anchored on ZrO_2 or TiO_2 surfaces showed no measurable spectral changes with respect to the solution spectra. IR measurements of **1**−**4** bound to TiO_2 revealed a single C═O stretch at ~1720 cm^{-1}.[28]

The PL decays of the sensitizers in acetonitrile solutions followed single-exponential kinetics, and the excited-state lifetimes are listed in Table 1, together with the PL quantum yields. The PL lifetimes for the phen-based tripodal sensitizers **1** and **3** (1.4 and 1.0 μs) were comparable to the PL lifetime of $Ru(bpy)_2(phen)^{2+}$ (1.2 μs). The PL lifetimes of bpy-based tripodal sensitizers **2** and **4** (2.0 and 2.2 μs) however, were considerably longer than that of $Ru(bpy)_3^{2+}$ (800 ns). The PL lifetimes for the two model complexes, phen-based **5** and bpy-based **6**, were nearly identical (~1.1 μs), and the latter compound has a notably high emission quantum yield.

Time-resolved PL decays for the tripods bound to ZrO_2 and TiO_2 were nonexponential and were well described by a parallel first- and-second-order kinetic model, eq 6.[29]

$$\mathrm{PLI} = \frac{Ck_1 \exp(-k_1 t)}{k_1 + k_2 C - k_2 C \exp(-k_1 t)} \qquad (6)$$

Here C is the excited-state concentration, k_1 is the first-order rate constant, and k_2 is the observed second-order rate constant. Typical data are shown in Figure 4 for [$Ru(bpy)_2(C\text{-}tripod\text{-}phen)^{2+}$] (**4**) on TiO_2 and ZrO_2 with surface coverages near saturation, approximately 2×10^{-8} mol/cm^2. The first-order rate constants on TiO_2 and ZrO_2 were 1.6×10^6 and 6.9×10^5 s^{-1}, respectively, while the second-order components were 4.3×10^7 and 3.0×10^6 s^{-1}, respectively. Consistent with previous studies for $Ru(deeb)(bpy)_2^{2+}/TiO_2$,[29] the first-order rate constant was typically $k_1 = (3 \pm 2) \times 10^6$ s^{-1}, and the second-order component was $k_2 = (9 \pm 5) \times 10^7$ s^{-1}.

Transient Absorption. The spectral features of the transient absorption spectra of **1**−**4** in acetonitrile solution and on

(28) (a) Deacon, G. B.; Phillips, R. J. *Coord. Chem. Rev.* **1980**, *33*, 227. (b) Umpathy, S.; Cartner, A. M.; Parker, A. W.; Hester, R. E. *J. Phys. Chem.* **1990**, *94*, 1357. (c) Finnie, K. S.; Bartlett, J. R.; Woolfrey, J. L. *Langmuir* **1998**, *14*, 2744.
(29) Kelly, C. A.; Farzad, F.; Thompson, D. W.; Meyer, G. J. *Langmuir* **1999**, *15*, 731.

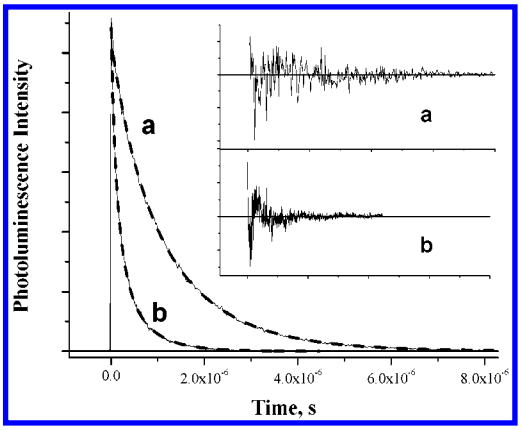

Figure 4. Normalized time-resolved photoluminescence decays for Ru(bpy)$_2$(C-tripod-bpy)(PF$_6$)$_2$ adsorbed on either (a) ZrO_2 or (b) TiO_2 (solid lines). Overlaid are fits to the parallel first- and second-order models (dashed lines). Inset: Residuals for fits. The samples were illuminated with pulsed 460 nm light.

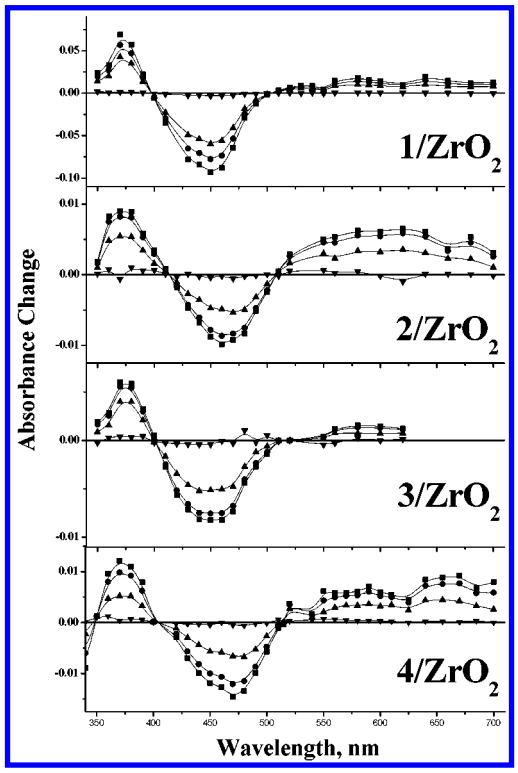

Figure 5. Time-resolved absorption difference (ΔA) spectra, obtained after pulsed 532.5 nm laser light excitation (~14 mJ cm^{-2}, 8 ns fwhm), of the tripodal complexes **1**−**4** bound to nanocrystalline ZrO_2 films in argon-purged CH_3CN electrolyte at 25 °C. The data were recorded at 10 ns (■), 100 ns (●), 500 ns (▲), and 5 μs (▼) delay after the laser pulse.

insulating ZrO_2 immersed in acetonitrile were the same within experimental error and were assigned to the MLCT excited state.

The rationale behind using ZrO_2 is that it is a metal oxide substrate that does not participate in interfacial electron-transfer processes and therefore affords MLCT excited-state characterization. Data for **1**−**4**/ZrO_2 are shown in Figure 5. The absorbance difference spectra for [Ru(bpy)$_2$(Ad-tripod-phen)$^{2+}$]*, [Ru(bpy)$_2$(C-tripod-phen)$^{2+}$]*, Ru(Ph-E-phen)$_3^{2+}$*, and Ru(bpy)$_3^{2+}$* are qualitatively very similar, with absorbance bands centered at ~310 and ~370 nm, an isosbestic point at ~397 nm, and weak bands beyond 600 nm. In contrast, the absorbance

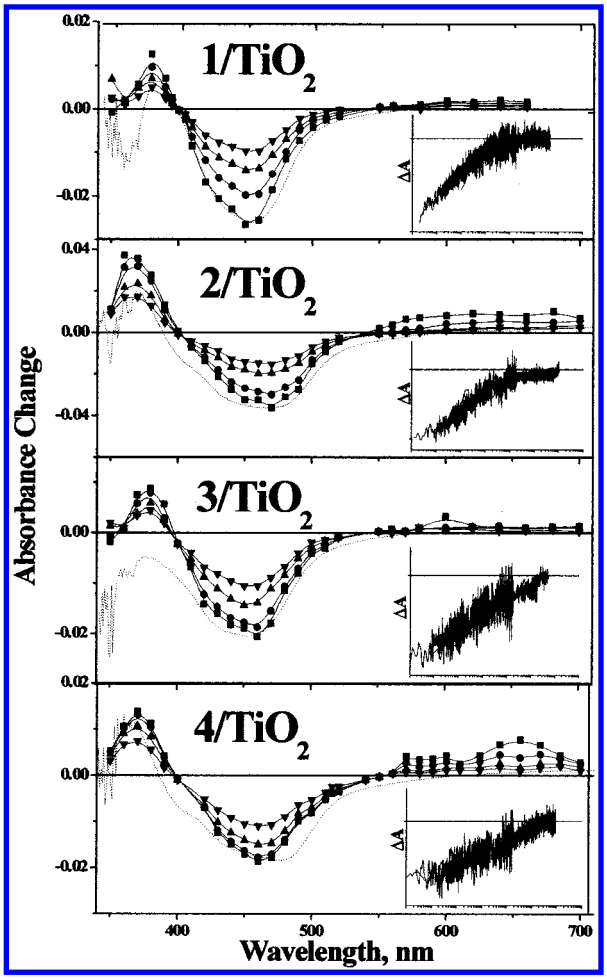

Figure 6. Time-resolved absorption difference (ΔA) spectra observed after pulsed 532.5 nm laser light excitation (~14 mJ cm^{-2}, 8 ns fwhm) of **1**−**4** bound to nanocrystalline TiO_2 films in CH_3CN. The data were recorded at 10 ns (■), 100 ns (●), 500 ns (▲), and 2 μs (▼) delays after the laser pulse. Overlaid are the absorption difference spectra from spectroelectrochemical experiments of sensitized TiO_2/FTO films (dashed line) obtained by subtracting the absorption spectrum of Ru^{II} from that of Ru^{III} (for details, see Supporting Information, Figure S3). Insets: Transient absorption signals of **1**/TiO_2, **2**/TiO_2, **3**/TiO_2, and **4**/TiO_2 monitored at 503, 509, 510, and 515 nm, respectively, after 532.5 nm laser excitation (~14 mJ cm^{-2}, 8 ns fwhm) displayed on a logarithmic time scale from 10^{-8} to 0.1 s.

difference spectra for [Ru(bpy)$_2$(Ad-tripod-bpy)$^{2+}$]* and [Ru(bpy)$_2$(C-tripod-bpy)$^{2+}$]* have a bleach centered at ~340 nm, absorbance bands centered at ~310 and ~380 nm, isosbestic points at ~325, 358, and ~405 nm, and intense absorption bands beyond 600 nm. The kinetics were first-order in acetonitrile solution and followed the parallel first- and second-order kinetic model on ZrO_2, with rate constants that agreed well with the time-resolved PL data.

Time-resolved absorption difference spectra of the four tripodal sensitizers bound to TiO_2 are shown in Figure 6. In all cases the normalized difference spectra recorded at different delay times were the same within experimental error. The spectra are assigned to an interfacial charge-separated state with an electron in TiO_2 and an oxidized Ru^{III} center, $Ru^{III}|TiO_2(e^-)$. The absorption difference spectra obtained from spectroelectrochemical data, i.e., Abs(Ru^{III}/TiO_2) − Abs(Ru^{II}/TiO_2), agree well with the difference spectra measured by transient absorption. At wavelengths greater than 600 nm, the spectroelectrochemical data underestimate the measured spectra slightly due

to the weak absorption of the $TiO_2(e^-)$. Experimental procedures and data are provided in the Supporting Information and in Figure S3.

The recovery of the ground-state absorption spectra, measured at a ground-excited-state isosbestic point, are shown as insets in Figure 6. The solid lines superimposed on the kinetic data represent fits to a sum of two second-order equal concentration processes (bi-second order), eq 7[4]

$$\Delta A = \frac{\Delta A_0 - \Delta A_s}{1 + (k_f/\Delta\epsilon l)t(\Delta A_0 - \Delta A_s)} + \frac{\Delta A_s}{1 + (k_s/\Delta\epsilon l)t(\Delta A_s)} \quad (7)$$

where ΔA is the absorbance change at time t, $\Delta\epsilon$ is the molar extinction coefficient, l is the optical path length, ΔA_o is the initial amplitude (equal to the sum of the contributions from the fast and slow components), k_f is the recovery rate constant for the fast component, ΔA_s is the amplitude of the slow component, and k_s is the recovery rate constant of the slow component. Typical observed rate constants for charge recombination for the two components (in units of absorbance) are 4×10^8 and 5×10^6 s^{-1}, respectively. The rates were independent of the tripodal sensitizer studied and were, within experimental error, the same as those observed for $Ru(bpy)_2(deeb)^{2+}/TiO_2$. The weights of the two components, ca. 70% and 30% for the fast and slow components, respectively, were also independent of the sensitizer. Conversion of the rate constants to units of concentration is difficult due to the heterogeneity of the sample and the resulting ill-defined nature of the optical path length, l.

Discussion

The synthetic methodologies described have allowed us to prepare a new class of molecular sensitizers, with novel semirigid tripodal ligands for binding to metal oxide surfaces.[10] These synthetic procedures can be extended to other sensitizers and can be used to control the coupling between the sensitizer and the semiconductor. The excited-state properties of tripods **1**−**4** anchored to colloidal ZrO_2 thin films as well as their electron-transfer dynamics on nanocrystalline (anatase) TiO_2 thin films provide insights into sensitizer−sensitizer and sensitizer−surface electronic interactions. Below we discuss the implications of the photophysical and electron-transfer behavior and compare it with recent literature reports.

1. Photophysical Behavior. The absorption and emission spectra of the surface-bound tripodal sensitizers **1**−**4** immersed in acetonitrile are, within experimental error, the same as those measured in fluid acetonitrile solution. This behavior is indicative of weak electronic coupling between the sensitizer and the semiconductor, and it differs considerably from that observed for inorganic coordination compounds bound to semiconductors through the dcb or the deeb ligand.[3] For instance, in the case of $Ru(deeb)(bpy)_2^{2+}$, the semiconductor surface and acid−base surface chemistry have a significant effect on the absorption and emission (Table 4).[30,34] Therefore, the tripodal sensitizers will be very useful to study excited states that are weakly coupled to the semiconductor surface.

Table 4. Comparison of Photophysical Properties for $Ru(bpy)_2(C\text{-}Tripod\text{-}bpy)^{2+}$ (**4**) and $Ru(bpy)_2(deeb)^{2+}$ in CH_3CN Solution and Bound to TiO_2

sensitizer	λ_{abs} (nm)	λ_{PL} (nm)	$E_{1/2}(Ru^{II/III})$ (V)	$E_{1/2}(Ru^{III/II*})$ (V)
4	461	655	1.32	−0.81
4/TiO_2	461	660	1.34	−0.78
$Ru(bpy)_2(deeb)^{2+}$	475	690	1.39	−0.62
$Ru(bpy)_2(deeb)^{2+}/TiO_2$	487	704	1.35	−0.76

Localization of the MLCT Excited State. Time-resolved resonance Raman experiments have demonstrated that the excited state of Ru^{II}-polypyridine complexes are localized on one ligand in the metal-to-ligand charge-transfer (MLCT) excited state on a nanosecond time scale.[31] DeArmond correlated spectroscopic and electrochemical data on heteroleptic Ru^{II} compounds and has convincingly shown that the first ligand reduced is the "optical" orbital relevant to the photoluminescent MLCT excited state at room temperature.[32] Based on DeArmond's correlation, the electrochemical data reported here are consistent with the excited state being localized on the surface-bound tripodal ligand for all compounds studied. The phenylethynyl substituent is electron withdrawing and lowers the π^* orbitals and reduction potential relative to those of unsubstituted bpy or phen ligands.[26] Furthermore, for bpy-based tripodal sensitizers $Ru(bpy)_2(Ad\text{-}tripod\text{-}bpy)^{2+}$ and $Ru(bpy)_2(C\text{-}tripod\text{-}bpy)^{2+}$, the absorbance and PL spectra are significantly red-shifted relative to that observed for $Ru(bpy)_3^{2+}$, consistent with the bpy-based tripodal ligand being lower in energy. A comparison of the excited-state absorption difference spectra of the tripodal sensitizers with other Ru^{II}-polypyridine complexes also reveals that the excited state is localized on the tripodal ligand. An interesting observation is that the bpy-based tripods give rise to longer excited-state lifetimes than do the phen-based tripods, despite the fact that the bpy compounds have a smaller energy gap.

Excited-State Relaxation Kinetics. An important difference between the excited states of the tripodal sensitizers in fluid solution relative to those attached to metal oxide surfaces is that, in the case of **1**−**4**/ZrO_2 and **1**−**4**/TiO_2, relaxation kinetics are nonexponential. Tripods **1**−**4** bound to the ZrO_2 and TiO_2 surfaces are well described by a parallel first- and second-order kinetic model. The appearance of a second-order component in the excited-state relaxation is indicative of excited state−excited state annihilation processes that result from fast intermolecular energy transfer (k_{EnT}) across the metal oxide interface (Scheme 3).[29] Direct evidence for intermolecular energy transfer has been previously reported for Ru^{II} and Os^{II} sensitizers bound to nanocrystalline TiO_2.[33] The observed second-order rate constant is a function of the excited-state concentration that is unknown under these experimental conditions. Nevertheless, the appearance of the second-order process reveals significant excited-state interaction between the surface-bound tripodal compounds.

2. Electron Transfer. Electron-transfer processes can be quantified in considerable molecular detail in the case of

(30) (a) Giordano, P. J.; Bock, C. R.; Wrighton, M. S.; Interrante, L.; Williams, R. F. X. *J. Am. Chem. Soc.* **1977**, *99*, 3187. (b) Ferguson, J.; Mau, A. W.-H.; Sasse, W. H. F. *Chem. Phys. Lett.* **1979**, *68*, 21. (c) Shimidzu, T.; Iyoda, T.; Izaki, K. *J. Phys. Chem.* **1985**, *89*, 642. (d) Mesmaeker, A. K.-D.; Jacquet, L.; Nasielski, J. *Inorg. Chem.* **1988**, *27*, 4451. (e) Nazeeruddin, M. K.; Kalyanasundaram, K. *Inorg. Chem.* **1989**, *28*, 4251. (f) Nazeeruddin, M. K.; Zakeeruddin, S. M.; Humphry-Baker, R.; Jirousek, M.; Liska, P.; Vlachopoulos, N.; Shklover, V.; Fischer, C.-H.; Grätzel, M. *Inorg. Chem.* **1999**, *38*, 6298.

(31) Dallinger, R. F.; Woodruff, W. H. *J. Am. Chem.* Soc. **1979**, *101*, 4391.
(32) DeArmond, M. K.; Hanck, K. W.; Wertz, D. W. *Coord. Chem. Rev.* **1985**, *64*, 65.
(33) Farzad, F.; Thompson, D. W.; Kelly, C. A.; Meyer, G. J. *J. Am. Chem.* Soc. **1999**, *121*, 5577.

Scheme 3

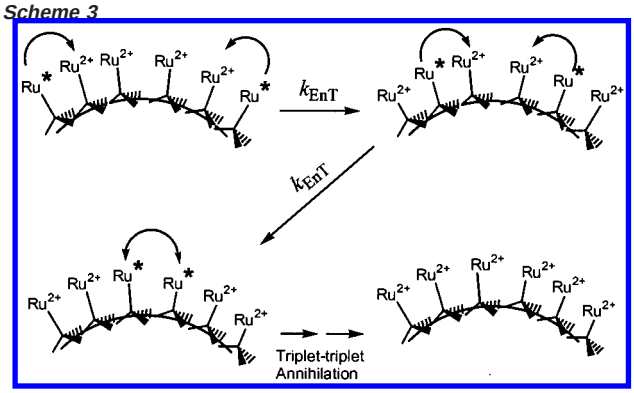

mesoporous TiO_2 films, which can be characterized both spectroscopically and electrochemically.[3] The tripodal linker reported here provides a more well-defined semiconductor−molecular distance and, in some cases, orientation than has been previously possible. For instance, in the case of *cis*-Ru(dcb)$_2$(NCS)$_2$, at most three of the four carboxylic acid groups can simultaneously interact with the semiconductor surface, resulting in a distribution of possible surface orientations.[3] The single asymmetric CO stretch in the IR spectrum of the surface-bound tripods (Table 3) indicates that all three carboxylic acid groups interact with the surface in an equivalent manner and are consistent with the idealized geometry of attachment shown in Figure 1b.[28] It was therefore of interest to quantify molecular electron-transfer processes with this new class of photosensitizers. Below we discuss our results on three types of electron-transfer processes and contrast them with previously published work.

Intermolecular Charge Transfer. We and others have found that redox-active molecules bound to mesoporous nanocrystalline TiO_2 films can be electrochemically oxidized and reduced in a reversible fashion.[27] Since the reduction potentials of the molecules exist near mid-band gap, the process does not involve the valence or conduction bands of the semiconductor. Instead, the accepted mechanism involves initial oxidation of compounds bound to the tin oxide substrate followed by intermolecular charge transfer across the nanoparticle surfaces, as shown in Figure S4 (Supporting Information). For the entire film to be oxidized, this mechanism requires electronic communication between all the surface-bound complexes. In fact, Grätzel and co-workers have quantified the percolation threshold necessary for complete oxidation of amines bound to related TiO_2 films.[27b] Chronoamperometry experiments with optical detection have allowed the apparent diffusion coefficient for intermolecular hopping with $Ru^{III/II}(bpy)_2(dcb)^{3+/2+}/TiO_2$ to be quantified, $D_{app} = 1.4 \times 10^{-9}$ cm^2/s in 0.1 M $TBAPF_6$ acetonitrile.[27c]

In previous work, an unexpected ionic strength dependence for intermolecular electron hopping was discovered.[34] The presence of small cations, such as H^+ or Li^+, at the TiO_2 interface, results in more rapid and efficient intermolecular charge transfer. These observations suggested that previously reported apparent diffusion coefficients might, at least in part, reflect the rate of counterion movement. Ion motion may be significantly influenced by specific surface adsorption effects, and it was therefore of interest to quantify these processes with the tripodal sensitizers, which have the Ru centers located ∼17 Å from the surface.

The values of D_{app} abstracted from the Cottrell equation with nearly saturated surface coverages were 10^{-11} cm^2/s for reduction and oxidation of the tripods. Measurements for Ru(bpy)$_2$(dcb)$^{2+}$/TiO_2 also gave $D_{app} \approx 10^{-11}$ cm^2/s, indicating that intermolecular charge-transfer rates are not significantly influenced by the presence of the tripodal ligands or the increased distance from the semiconductor surface. The footprint of the tripodal ligands (∼70 Å^2) is comparable in size to those of Ru^{II} tris-chelates, and we anticipate that the packing density, and hence sensitizer−sensitizer distance, will be similar to those observed for other Ru^{II} sensitizers. Therefore, the values of D_{app} should not be influenced by the sensitizer−sensitizer distance, and the fact that they are insensitive to the tripodal linkage and spacer suggests that proximity to the surface and specific ion adsorption are not significant factors under these experimental conditions.

Charge Separation. Interfacial charge separation at dye-sensitized TiO_2 surfaces has been the subject of many studies.[3] For Ru^{II} sensitizers, electron transfer generally occurs from the π^* orbitals of a coordinated dcb ligand to the empty states of the semiconductor, and there is some spectral evidence that the dcb ligands provide strong electronic coupling to the semiconductor surface.[3] Recent ultrafast spectroscopic studies have revealed femtosecond electron injection rates from Ru^{II}* excited states under a variety of experimental conditions.[35]

In contrast to other inorganic sensitizers, the absorption and emission properties of **1**−**4** in fluid solution and **1**−**4**/MO_2 are, within experimental error, the same, consistent with weak electronic coupling to the surface. We therefore expect charge separation to occur from the thermally equilibrated excited state localized on the surface-bound tripodal ligand for **1**−**4**. In all cases, the rate constant for charge separation was faster than could be time-resolved with our instrumentation, $k_{cs} > 10^8$ s^{-1}. Since the radiative and nonradiative rate constants for these compounds in fluid solution are several orders of magnitude slower, ∼10^4 and 10^5 s^{-1}, respectively, a quantum yield for electron injection near unity would be expected for an injection rate of ∼10^8 s^{-1}. This expectation is consistent with the transient absorption data that reveal no clear evidence for excited states for the compounds bound to TiO_2 (see Supporting Information).

Electron transfer from excited states that are weakly coupled to the semiconductor have been previously reported.[36] Researchers have introduced $(CH_2)_n$ spacers between the carboxylic acid groups and a bpy ligand to attenuate the electronic coupling to the surface.[8] Lian and co-workers quantified the decrease in excited-state electron injection rate constant as the alkyl spacer increased in two complexes of the type *fac*-Re(CO)$_3$Cl(L), where L = 4,4′-[HO_2C-$(CH_2)_n$]-2,2′-bpy, with $n = 1$ and $n = 3$.[8b] The injection rate decreased by a factor of 12.6 as n increased from $n = 1$ (5.3×10^{10} s^{-1}) to $n = 3$ (4.2×10^9 s^{-1}). If the flexible

(34) Qu, P.; Meyer, G. J. *Langmuir* **2001**, *17*, 6720.

(35) (a) Tachibana, Y.; Moser, J. E.; Grätzel, M.; Klug, D. R.; Durrant, J. *J. Phys. Chem.* **1996**, *100*, 20056. (b) Hannappel, T.; Burfeindt, B.; Storck, W.; Willig, F. *J. Phys. Chem. B* **1997**, *101*, 6799. (c) Heimer, T. A.; Heilweil, E. J. *J. Phys. Chem. B* **1997**, *101*, 10990. (d) Ellingson, R. J.; Asbury, J. B.; Ferrere, S.; Ghosh, H. N.; Sprague, J. R.; Lian, T.; Nozik, A. J. *J. Phys. Chem. B* **1997**, *101*, 6455. (e) Benko, G.; Kallioinen, J. E.; Korppi-Tommola, J. E. I.; Yartsev, A. P.; Sundstrom, V. *J. Am. Chem. Soc.* **2002,** *124*, 489.

(36) Qu, P.; Thompson, D. W.; Meyer, G. J. *Langmuir* **2000**, *16*, 4662.

spacer was fully extended for the $n = 3$ case, the approximate distance from the pyridyl nitrogen to the oxygen in the carboxylic acid would be ~6.5 Å. Extrapolation of these data to distances of ~17 Å would suggest that the rates for charge separation should be time resolved with ~10 ns time resolution. However, the energetics for the Re^{I} excited states are different than those for the heteroleptic Ru^{II} compounds. In addition, the excited states in **1**−**4** may delocalize over the phenylethynyl spacer, resulting in a significantly decreased charge separation distance compared to that for the Re compounds. Studies with a homologous series of tripodal sensitizers as a function of distance are under way in our laboratories and will provide valuable insights into this behavior.

Charge Recombination. Recombination of the injected electron with the oxidized dye required milliseconds for completion, a result that is consistent with previous studies of other Ru^{II} sensitizers.[3] The recombination process follows second-order kinetics with rate constants that are independent of the tripod studied. Since the $Ru^{III/II}$ potentials and the semiconductor-Ru^{III} distance are very similar for all four tripods, the fact that the rate constants are the same is not surprising. However, we had previously noted that the rate of charge recombination was faster for $Ru(bpy)_2(Ad\text{-}tripod\text{-}bpy)^{3+}|TiO_2(e^-)$ than for $Ru(bpy)_2(dcb)^{3+}|TiO_2(e^-)$ under conditions of constant irradiance, temperature, and electrolyte.[11] In examining a larger data set and the newly synthesized tripods reported here, we again find that the time scale, and hence rate, for charge recombination is consistently slower for $Ru(bpy)_2(dcb)^{3+}|TiO_2(e^-)$. However, the weighted-average observed rate constants abstracted from the bi-second-order model are, within a factor of 3, the same for all the tripods and for $Ru(bpy)_2(dcb)^{3+}|TiO_2(e^-)$. Uncertainty in the path length and extinction coefficients preclude us from quantifying the true second-order rate constants, and a small difference in $\Delta\epsilon$ at the isosbestic point for $Ru(bpy)_2(dcb)^{3+}|TiO_2(e^-)$ could account for the different rate. We therefore conclude that the charge recombination rate constants for the tripods and $Ru(bpy)_2(dcb)^{3+}|TiO_2(e^-)$ are, within experimental error, the same.

Previous work in our[37] and in others'[38] laboratories has established that the charge recombination rate constants can be remarkably insensitive to the apparent thermodynamic driving force, the sensitizer geometry, the number of carboxylic acid groups, and the nature of the metal center (Ru, Os, or Re).[37] The results suggested that the charge recombination was rate limited by a process other than interfacial charge recombination. Nelson and Durrant have provided strong evidence that diffusion of the injected electron in the TiO_2 film is the rate-limiting process.[38] If diffusion is rate-limiting here, then slowing down charge recombination by further increasing the semiconductor−Ru^{III} distance should ultimately lead to a change in the mechanism for charge recombination. Studies of this type are underway in our laboratories.

Conclusions

Four Ru^{II}-polypyridyl compounds (**1**−**4**) containing tripodal ligands were synthesized and characterized for photophysical and electron-transfer studies at nanoparticle interfaces. The Ru centers are ~15−17 Å from the surface and are attached through a bridge that is not completely conjugated. As a result, the redox and steady-state optical properties of the compounds are unchanged upon attachment to the nanoparticles, suggesting weak sensitizer−surface electronic coupling. This behavior has not been previously reported for other Ru^{II} sensitizers.[3] Therefore, the tripodal compounds are useful to prepare sensitizers that are not altered by surface chemistry. Whereas the structural differences among **1**−**4** are relatively small, this first series provides a useful data set for tripodal sensitizers that can be compared to data available for other Ru^{II}-polypyridine dyes.[3] Systematic variations of the spacer and the sensitizer and numerous other structural changes will be explored in future studies.

Acknowledgment. The Division of Chemical Sciences, Office of Basic Energy Sciences, Office of Science, U.S. Department of Energy, and the Petroleum Research Fund (ACS-PRF 35081-G5) are gratefully acknowledged for research support by E.G. G.J.M. acknowledges the Division of Chemical Sciences, Office of Basic Energy Sciences, Office of Science, U.S. Department of Energy.

Supporting Information Available: Detailed synthetic procedures for the synthesis of **1**−**6**, the method for TiO_2 nanoparticles preparation, a description of the spectroelectrochemical oxidation of **1**−**4**/TiO_2/FTO, cyclic voltammograms for **1**−**4**, solution absorption spectra for **1**−**4**, and a schematic for the electron hopping mechanism by which oxidation of sensitized TiO_2 films occurs (PDF). This material is available free of charge via the Internet at http://pubs.acs.org.

JA025840N

(37) Hasslemann, G. M.; Meyer, G. J. *J. Phys. Chem. B* **1999**, *103*, 7671.
(38) (a) Nelson, J. *Phys. Rev. B* **1999**, *59*, 15374. (b) Nelson, J.; Haque, S. A.; Klug, D. R.; Durrant, J. R. *Phys. Rev. B* **2001**, *63*, 205321.
(39) Vlcek, A. A.; Dodsworth, E. S.; Pietro, W. J.; Lever, A. B. P. *Inorg. Chem.* **1995**, *34*, 1906.
(40) Bugnon, P.; Hester, R. E. *Chem. Phys. Lett.* **1983**, *102* (6), 537.
(41) De Cola, L.; Barigeletti, F. *Helv. Chim. Acta* **1988**, *71*, 733.